AUTHORS' REVIEW

Calculation of the Jahn–Teller parameters with DFT•

MATIJA ZLATAR[1#] and MAJA GRUDEN[2*#]

[1]*University of Belgrade-Institute of Chemistry, Technology and Metallurgy, Department of Chemistry, Njegoševa 12, Belgrade, Serbia and* [2]*University of Belgrade, Faculty of Chemistry, Studentski trg 12–16, Belgrade, Serbia*

Abstract: In this review, a density functional theory (DFT) procedure is presented to calculate the Jahn–Teller (JT) parameters in a non-empirical way, which does not depend on the system at hand. Moreover, the intrinsic distortion path (IDP) model that gives further insight into the mechanism of the distortion is presented. The summarized results and their comparison to experimentally estimated values and high-level *ab initio* calculations, not only prove the good ability of the used approach, but also provide many answers to the intriguing behavior of JT active molecules.

Keywords: vibronic coupling; density functional theory; intrinsic distortion path; distortion; transition metal complexes; organic ions and radicals.

CONTENTS

1. INTRODUCTION
2. METHODOLOGY
3. RESULTS AND DISCUSSION
4. CONCLUSIONS
5. REFERENCES

1. INTRODUCTION

Since its discovery more than 80 years ago, the Jahn–Teller (JT) effect[1] has drawn much attention in the scientific community, usually among scientists described as: "When a baby cries without anyone knowing why, we say - these are the teeth. Similarly, in the chemistry of transition metal compounds, when experimental phenomenon cannot be interpreted easily, it is often attributed to the Jahn–Teller effect. Moreover, the Jahn–Teller effect is simultaneously a source

---

of comfort and of anxiety. Comfort because it is still there as a last resort to explain a result. Anxiety because it is challenging to reliably prove it, without remaining ambiguity".[2] A witty quotation, translated from French, reflects the difficulties and challenges in both experimental and computational determination of the JT effect. It echoes another common misapprehension – that the JT effect is related only to transition metal complexes, which is certainly not the case. The JT effect also occurs in highly symmetric open shell molecules, such as the cyclopentadienyl radical, benzene cation, fullerene ions, to name a few. After the Nobel Prize for physics in 1987,[3] when its importance in high-Tc superconductivity was highlighted, it became more apparent that this phenomenon is not only of fundamental interest, but also applicable in many areas of chemistry and physics.[4]

The JT theorem states that in a non-linear molecule with a degenerate ground state, structural distortion must occur, which removes the degeneracy, lowers the symmetry and stabilizes the system. In linear molecules because of symmetry constraints degenerate, electronic states cannot couple with appropriate vibrations. However, these molecules can still be distorted, as described by the Renner–Teller (RT) effect.[5] Although here the JT effect is mentioned first, it is noteworthy that historically it was preceded by the discovery of the RT effect.[5] A requirement that a molecule must be in a degenerate electronic state to be a subject of the JT and RT effects is excluded in the pseudo-Jahn–Teller (PJT) formalism.[4,6,7] All these effects belong to so-called "vibronic interactions."[4,8,9] Vibronic coupling is a quantum mechanical description of the influence of vibrations on the electronic structure, and *vice versa*. These effects are the origin of various molecular properties, such as colossal magnetoresistance,[10,11] high-Tc superconductivity,[3,12] nonconventional superconductivity,[13] single-molecule transport,[14] ferroelectricity,[4,15] spin-crossover[16] and dynamics.[9] They are essential in the design of single molecular magnets.[17–19] The vibronic coupling is responsible for the observation of symmetry-forbidden transitions in spectroscopy,[20] conical intersections in photochemistry, and is indispensable for understanding the spectroscopy of linear molecules.[21–26] The cause of any structural distortion of a polyatomic system is due to the JT, RT, PJT effect, or their combination.[4,7,27] Thus, the shape of molecules, both linear[28] and non-linear,[29,30] as well as solids,[31] is explained within the framework of vibronic coupling theories. The coupling of electronic structure and nuclear movements is also essential for a proper understanding of chemical reactions.[32–36]

Due to the coupling of electronic and vibrational motions, the Born–Oppenheimer (BO) approximation fails at the point of electronic degeneracy. That was one of the main reasons why it has been wrongly assumed that first principle calculations cannot be applied to analyze JT or RT effects. However, the breakdown of the BO approximation brings an apparent paradox. JT type effects

emerge because of the non-validity of the BO approximation, but the effects as such would not exist if the BO approximation is not used in the first place. The JT effect exists only in the realm of the BO approximation. Without the BO approximation, we do not have a picture of the molecule and there would be no sense in discussing a distortion of a molecular structure. Standard concepts in theoretical chemistry, such as force or force constants, would lose their meaning. Nonetheless, a perturbation approach restores the BO approximation. A Hamiltonian is written as a Taylor series in nuclear coordinates. Coefficients in the polynomial expression of an adiabatic potential energy surface are the vibronic coupling constants, and they quantify the strength of the coupling between the electronic structure and nuclear displacements.[4] These coefficients are complicated integrals that have physical interpretation, such as force and force constant at a high symmetry configuration.[4] Conventional computational methods could still be used if the adiabatic potential energy surface is accurately determined, which is nowadays possible with most computational methods. Many studies confirmed the excellent ability of both wave-function based methods and density functional theory (DFT) based methods to analyze vibronic coupling.[4,37] Typical studies do not calculate the vibronic coupling constants directly, but the calculated adiabatic potential curves along the distortion are fitted to the polynomial expression that resulted from the vibronic coupling model.[30,38–41] Computational studies enabled a more in-depth insight into the properties of JT active compounds and the understanding of many manifestations of the JT effect.

In the last decades, DFT has emerged as the mainstream among computational methods, preferable because it gives a good compromise between accuracy and computational time. The theory of DFT is well documented,[42–48] and here, just a brief explanation is given in a non-mathematical way of what the density functional theory is and how it can be applied to analyze the JT effect. In its theory, the DFT gives the exact energy of the system as a method of obtaining a solution to the Schrödinger equation of a many-body system, using electron density. The Hohenberg–Kohn theorem[49] asserts that the density of any system determines all ground-state properties of the system, so the total ground state energy of a multi-electron system is a functional of the density. Consequently, if the electron density functional is known, the exact total energy of the system is given. In practical computational work, as there is still no universal functional, approximations have to be made, leading to many functionals designed for certain properties.[43,50]

There is a controversy in the literature whether DFT can be used for the analysis of the JT effect,[51–53] as the original Hohenberg–Kohn theorems[49] were formulated only for non-degenerate ground states in the absence of a magnetic field. However, the second reformulation of this theorem gives formally proof that the DFT can handle degenerate states.[54,55] This issue is also elaborated

within the sub-system ensemble DFT,[56,57] the spin-restricted ensemble-referenced Kohn–Sham (KS) DFT,[58] the nonadiabatic generalization of DFT[59] and the sign-change in DFT.[60] Additionally, DFT naturally encompasses the mechanism of the JT effect.[61,62] Electron density must be totally symmetric in a point group of a molecule. This is not possible if the orbitals belonging to a degenerate irreducible representation (irrep) are not equally occupied. In such cases, non-totally symmetric density will lead to non-isotropic forces on nuclei, driving the distortion to the molecular structure with lower point-group than the initial one. A molecular structure with degenerate electronic states in a high-symmetry (HS) point group is, therefore, not a stationary point. In the case of the PJT effect, the change in the distribution of electrons along a distortion is accompanied by a lowering of the force constant of the high-symmetry configuration.[4,7,29,63] Admittedly, from a practical point of view, care should be taken when dealing with JT type effects with DFT.[37,64] A pragmatic way for a detailed calculation of the JT effect was developed by Daul *et al.*,[37,64,65] and it has been successfully applied for the analysis of many JT active molecules.[64–75]

2. METHODOLOGY

Within vibronic coupling theory, Hamiltonian, $\mathcal{H}$, is expanded as a Taylor series around the HS molecular structure, along the normal modes, Q_i:

$$\mathcal{H} = \mathcal{H}_0 + \Sigma_i(\partial\mathcal{H}/\partial Q_i)Q_i + 1/2\Sigma_{ij}(\partial^2\mathcal{H}/(\partial Q_i\partial Q_j))Q_iQ_j + \ldots \tag{1}$$

where $\mathcal{H}_0$ is the Hamiltonian for the reference nuclear configuration, and the sum that follows it is the JT or vibronic Hamiltonian, W. The adiabatic potential energy surface for an *f*-fold degenerate electronic state takes the form

$$E_k = 1/2 \, \Sigma_i K_i Q_i^2 + \varepsilon_k \tag{2}$$

where $k = 1,2,\ldots f$, and K_i is the force constant for the vibration Q_i and ε_k are the roots of the secular equation:

$$|W - \varepsilon I| = 0 \tag{3}$$

W is an *f×f* vibronic matrix, and I is a unit matrix of the same dimensions. The matrix elements of the vibronic operator are the vibronic coupling constants. For instance, the linear vibronic coupling constant has the form $F_{i,k} = <\Psi_k|\partial\mathcal{H}/\partial Q_i|\Psi_k>$, where Ψ_k is the wavefunction belonging to the *k*-th component of the degenerate state. Group theory can be used to judge whether these matrix elements are different from zero. Irrep of the JT active normal modes must belong to the same representation as the symmetric direct product of the components of the degenerate electronic state, to have a linear coupling constant different from zero.

For example, in the case of the JT active Sb_4^-, electronic ground state in square planar (D_{4h}) configuration is ^2E_g, and vibrations that belong to B_{1g} and B_{2g} irreps distort the structure to rhombus and rectangle, respectively. Both distorted structures belong to the D_{2h} point group. The adiabatic potential energy surface of Sb_4^- in the space of two JT active vibrations is depicted in Fig. 1. The parameters used to construct the surface were obtained by DFT.[70]

Another example is the VCl_4 tetrahedral molecule (T_d point group) with an E ground electronic state coupled with double degenerate vibrations also belonging to E irrep. Distortion lowers the symmetry to D_{2d}, and the degenerate state splits into $^2A_1$ and $^2B_1$. The adiabatic

potential energy surface has the famous wrapped "Mexican-hat-like" form, with three equivalent minima and three equivalent transition states, Fig. 2.
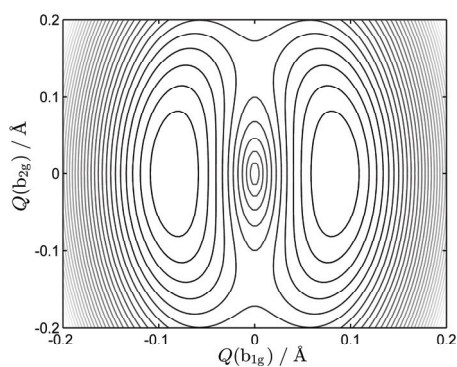

Fig. 1. Contour plot of the adiabatic potential energy surface of Sb_4^- in the space of JT active b_{1g} and b_{2g} normal modes. Minima have rectangular and transition states rhombic geometries.[70]
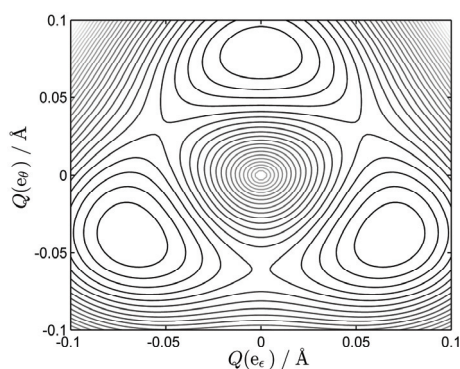

Fig. 2. Contour plot of the adiabatic potential energy surface of VCl_4 in the space of two components of the JT active e vibration. Minima have $^2A_1$, and transition states $^2B_1$ state.[64]

Vibronic coupling constants determine the shape of the adiabatic potential energy surface (Figs. 1 and 2). However, from a computational perspective, it is more natural to define it with the JT stabilization energy (E_{JT}), warping barrier (Δ) and JT radius (R_{JT}). A qualitative cut through the adiabatic potential energy surface, along the JT active distortion Q_a, is given in Fig. 3, indicates how this set of JT parameters define the adiabatic potential energy surface of JT active molecules. The meaning of the parameters is clear – the value of E_{JT} gives the energy stabilization due to the distortion, the energy difference between the minimum (min in Fig. 3) and transition state (TS in Fig. 3) is Δ, and the direction and magnitude of the distortion are given with R_{JT}.

The set of JT parameters, Fig. 3, is, at least in principle, easy to determine from the first principle calculations. To obtain the JT parameters, one needs to know the proper geometry and, consequently, the energy of the HS configuration, as well as the geometries and energies of the distorted, electronically non-degenerate low symmetry (LS) structures. Experimental determination of the parameters is less straightforward. One needs to fit the experimentally obtained results to the proposed model.

The procedure for calculating the JT parameters using DFT consists of three steps:[37,64]

1. Geometry optimization constraining symmetry to the HS point group. This yields a geometry of the high-symmetry configuration, with an electronic structure in which the electrons of degenerate orbitals are distributed equally over the components of the degenerate

irreps, *e.g.*, for e¹-configuration this will mean to place 0.5 electrons into each of the two (alpha) e-orbitals; for e³-configuration, 0.5 electrons will be in each of two beta e orbitals.

2. Performing a single-point calculation constraining the HS on the nuclear geometry and the LS on the electron density. This gives the energy of a Slater determinant with an integer electron orbital occupancy. It is necessary to evaluate the energies of all possible Slater determinants with integer electron occupations. In other words, all possible modes of occupation of the molecular orbitals need to be evaluated. This step is achieved by introducing an adequate occupation scheme of the molecular orbitals (MO).

3. A geometry optimization constraining the structure to the low-symmetry point group, with the proper occupancy of the KS orbitals. These calculations yield different geometries and energies that correspond to a minimum and a transition state on the adiabatic potential energy surface.
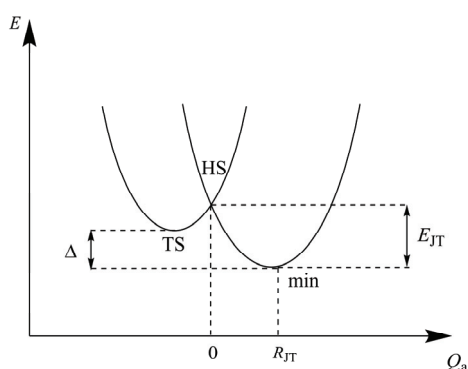

Fig. 3. Qualitative cross-section through the adiabatic potential energy surface, along the JT active distortion Q_a from the high-symmetry point (HS) toward the minimum (min) and transition state (TS); definition of the JT parameters: the JT stabilization energy (E_{JT}), the warping barrier (Δ) and the JT radius (R_{JT}).

This calculation scheme is schematically drawn in Fig. 4 for the calculation of the JT parameters in octahedral Cu(II) complexes. E_{JT} is the difference between the energies obtained in steps 2 and 3. As stated above, steps 2 and 3 are repeated for different combin-
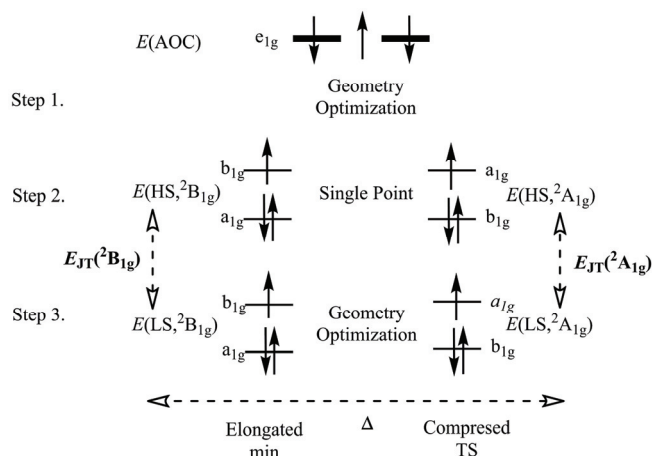

Fig. 4. DFT approach for the calculation of the JT parameters. The JT effect in an octahedral Cu(II) complex is taken as an example.

ations of electronic states in the LS point group. Hence there will be different E_{JT} for a minimum and transition state structures. The difference between the two E_{JT} values gives the warping barrier, Δ. R_{JT} is given by the length of the distortion vector between the high symmetry and the minimum energy configuration, *i.e.*, the difference in the geometries from step 1 and 3.

To avoid calculating the geometry and energy at the HS configuration, it is possible to use the energy of the vertical (Franck–Condon) transition, E_{FC}, from the LS distorted structures.[74] This energy is easily obtained by promoting the unpaired electron from the ground state to the first excited state for the ground state (LS) geometry. When anharmonicity is negligible, *i.e.*, in the linear and quadratic JT models, $E_{JT} = 4E_{FC}$.

The first step consists of the calculation with a non-integer electron configuration. Since MOs themselves have no physical meaning, using the partial occupation is just a way of obtaining the electron density of the A_1 symmetry in the HS point group. As the electron density is totally symmetric, it exerts the same force on all atoms. After geometry optimization in step 1, the total force is null. Passing from this configuration with fractional occupation numbers, to the one with integer occupation, in the second and third step, leads to a change in the electronic density responsible for the non-zero force. Distortion thus occurs because a change in the electronic density requires modifying the equilibrium geometry.[42,61] This is illustrated in Fig. 5, where the difference in electron densities between steps 2 and 1 for the case of $[CuF_6]^{4-}$ is depicted, together with the resulting force (calculated at the LDA//TZP level of theory). The resulting forces lead to tetragonal distortion and stronger equatorial bonds compared to the axial ones. Lowering of the symmetry in step 2 is necessary because this is the only way that the electron density is totally symmetric with integer occupations of the MOs.
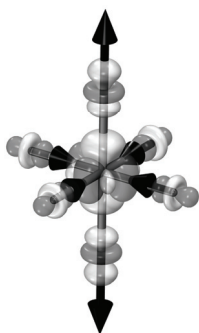

Fig. 5. Change of the electron density from the orbital configuration with fractional occupation to the one with integer occupation in the O_h configuration of $[CuF_6]^{4-}$. Light/dark color represents electron density depletion/concentration (iso-value 0.002 a.u). Forces on atoms are represented as black arrows.

Calculation of the Hessian at step 3 indicates the character of the stationary points – minimum or transition state. This correlates with the relative magnitudes of the two E_{JT}. Interestingly, it is possible to calculate the Hessian also in step 1, and all eigenvalues should be positive. This means that geometry from step 1 is the minimum for such an electronic configuration (with fractional occupation numbers). This nuclear configuration is a minimum structure (hypothetically) in the absence of the JT effect.

The JT parameters that are obtained from the calculations, Figs. 3 and 4, relate to the vibronic coupling constants.[4] However, the exact relations will depend on the vibronic coupling model used. For example, in the case of Sb_4^-, for each of the two JT active vibrations (b_{1g} and b_{2g}), Fig. 1, the relations are $E_{JT} = F^2/2K$ and $R_{JT} = F/K$, where F is the linear vibronic coup-

ling constant, and K is the force constant of the normal mode.[70] In the case of VCl_4, Fig. 2, second-order vibronic coupling is operational, and the relations are: $E_{JT} = F^2/2(K-|G|)$, $R_{JT}(\text{min}) = |F|/(K-2|G|)$, $R_{JT}(\text{TS}) = |F|/(K+2|G|)$, $\Delta = 4E_{JT}/(K+2|G|)$, where F, K and G are the linear vibronic coupling constant, the force constant and the quadratic vibronic coupling constants, respectively.[64]

It is worth mentioning that the calculated JT parameters are not very sensitive to the choice of exchange-correlation functional.[73] However, the JT parameters strongly depend on geometry. Hence the proper choice of the functional for the system at hand is of utmost importance. For organic molecules, this is not a difficult task, but for transition metal compounds particular caution (especially concerning spin states) is required.[76]

Further insight into what is occurring during distortion is based on the analysis of R_{JT}. It has already been mentioned that R_{JT} describes the direction and magnitude of the distortion. In the case of the triangular Na_3 cluster, it is represented by changing the angle.[40] In other simple cases, the distortion corresponds to the movements of nuclei along one normal mode that belongs to a non-totally symmetric irrep of the HS point group of a molecule. R_{JT} is then the magnitude of the distortion along that normal mode. In simple octahedral Cu(II) complexes often the following relation is used:[65] $R_{JT}^2 = \Sigma_i \, \delta d_i$, where $\delta d_i = d_i - d_0$, where d_i is the distance from the Cu(II) ion to the i-th ligand, and d_0 is the average metal–ligand distance. In more complex molecules, the JT distortion is a consequence of many active modes. The evaluation of the influence of different normal modes on the JT effect is a "multimode problem," and suitable models have to be employed to analyze the distortion.[4,37,41,77] The two most successful models for the analysis of the multimode problem are the "interaction mode"[41,78,79] and the "intrinsic distortion path" (IDP).[37,67,77]

The interaction mode[41,78,79] is a single, effective mode that is built as a linear combination of all the JT active normal modes of the HS configuration. Coefficients in this linear combination depend on the vibronic coupling constants of each mode, and the vibronic coupling model used. Typically, the interaction mode describes the straight-line path between the HS and LS geometries, $i.e.$, its direction coincides with the direction of R_{JT}. It is crucial to notice that the interaction mode is a reducible representation in the HS point group, while it belongs to the totally symmetric irreducible representation in the LS point group. The same is true for R_{JT}.

The essence of the IDP model[37,67,77] is to express the distortion along a model minimal energy path starting from the DFT, or the first-principle HS geometry, and ending in the LS minimum, or the LS transition state. The reference point in IDP is the LS configuration, and the energy surface is approximated to be harmonic, $i.e.$, quadratic in the LS vibrational modes. This model allows the determination of both the presence and contribution to the E_{JT} and R_{JT} of all normal modes involved. All totally symmetric normal modes in the LS configuration contribute to the distortion because IDP as a "reaction path" must be totally symmetric.[36] The analytical expression of the energy allows the total force at the HS point to be obtained directly. This force can be projected on either HS or LS normal modes. Knowing that the physical interpretation of the linear vibronic coupling constants is the force along an HS normal mode,[4] the IDP directly evaluates all the linear vibronic coupling constants.[77] The contributions of each mode along the path change, thus providing a very detailed picture of the mechanism of the distortion.

Both, interaction mode and IDP have their advantages and drawbacks, as discussed in the literature,[77] and reduce a multidimensional energy surface that is difficult to visualize to a simple cross-section.

3. RESULTS AND DISCUSSION

Using the procedure mentioned above, many JT active molecules were analyzed, ranging from small metal clusters and organic radicals to organo-metallic compounds and coordination compounds (Table I). All these molecules differ in the number of atoms, nature of the chemical bonding, symmetry of the distortion, range of the JT stabilization energy. However, in all cases, we obtained good agreement with experimentally evaluated values or high-level *ab initio* data.

TABLE I. Results of the DFT calculations performed to analyze the JT effect of a set of compounds, and comparison to the available reference values (ref.)

Molecule	Distortion	E_{JT}(DFT) cm^{-1}	Ref. (DFT)	E_{JT} (ref.) cm^{-1}	Ref.
VCl_4	$T_d \rightarrow D_{2d}$	50	37,64	30–80	80–83
Cu_3	$D_{3h} \rightarrow C_{2v}$	530	67	280–550	4
Na_3	$D_{3h} \rightarrow C_{2v}$	870	73	760–1160	40,84,85
Sb_4^-	$D_{4h} \rightarrow D_{2h}$	579	70	–	–
As_4^-	$D_{4h} \rightarrow D_{2h}$	840	70	–	–
$^\bullet C_5H_5$	$D_{5h} \rightarrow C_{2v}$	1235	37,66	1237	86
$C_6H_6^+$	$D_{6h} \rightarrow D_{2h}$	879	66	700–1000	87–89
$C_6H_6^-$	$D_{6h} \rightarrow C_{2v}$	1187	66	–	–
$^\bullet C_7H_7$	$D_{7h} \rightarrow C_{2v}$	853	66	1043–1374	90
C_{60}^+	$I_h \rightarrow D_{5d}$	600	77	557	91
C_{60}^-	$I_h \rightarrow C_{2h}$	300–315	92	280–600	4
$C_{20}H_{10}^+$	$C_{5v} \rightarrow C_s$	548–665	68	–	–
$C_{20}H_{10}^-$	$C_{5v} \rightarrow C_s$	404–540	68	952	93
$C_{24}H_{12}^+$	$D_{6h} \rightarrow D_{2h}$	287–401	68	484	94
$C_{24}H_{12}^-$	$D_{6h} \rightarrow D_{2h}$	290–410	68	645	94
$CoCp_2$	$D_{5h} \rightarrow C_{2v}$	870	67	1050	80,95
$MnCp_2$	$D_{5h} \rightarrow C_{2v}$	500	96	350	80,95
$[FeCp_2]^+$	$D_{5h} \rightarrow C_{2v}$	462	96	–	–
Pc^{3-}	$D_{4h} \rightarrow D_{2h}$	319–454	71	–	–
$MgPc^-$	$D_{4h} \rightarrow D_{2h}$	399–614	71	406	97
$MnPc$	$D_{4h} \rightarrow D_{2h}$	137–152	71	–	–
$[Cu(TACN)_2]^{2+}$	$D_3 \rightarrow C_2$	1790	98	1800	99
$[Ni(TACN)_2]^{3+}$ (low spin)	$D_3 \rightarrow C_2$	1504	98	1609	100
$[Co(TACN)_2]^{2+}$ (low spin)	$D_3 \rightarrow C_2$	1995	98	–	–
$[Co(TACN)_2]^{3+}$ (intermediate spin)	$D_3 \rightarrow C_2$	2168	98	–	–
$[Cu(en)_3]^{2+}$	$D_3 \rightarrow C_2$	2200	75	1800–2200	101
$[Cu(eg)_3]^{2+}$	$D_3 \rightarrow C_2$	1980	75	1620–2000	101
$[NiCl_3(Hdabco)_2]^+$	$D_3 \rightarrow C_2$	253	18	–	–

VCl$_4$ and Sb$_4^-$, Figs. 1 and 2, have already been mentioned. The modes that can contribute to the distortion are a$_1$ and e for VCl$_4$ and a$_{1g}$, b$_{1g}$ and b$_{2g}$ for

Sb_4^-. Totally symmetric modes do not change the symmetry. However, in principle, need to be taken into consideration since their vibronic coupling constants are not zero by symmetry. Our analysis based on the IDP model indicated that totally symmetric modes do not contribute to the distortion in these molecules.[37,70] Thus, the JT effect in VCl_4 is in essence an example of ideal, single mode JT distortion, and Sb_4^- is the simplest multimode problem. However, in Sb_4^- only one mode is responsible for the distortion to the minimum and the other one to the transition state. IDP is designed for more complicated situations[77] but is also perfectly suitable for these cases. IDP analysis justifies illustration of adiabatic potential energy surfaces for these molecules as depicted in Figs. 1. and 2. As_4^- is completely an analog to Sb_4^-.[70] Vibronic coupling constants for all three molecules were calculated by IDP, by their relation to the DFT obtained JT parameters, and by fit to the potential energy curves along the JT active normal modes. The results of the different approaches are consistent. DFT results for VCl_4 ($E_{JT} = 50$ cm^{-1})[37,64] are in good agreement with experimental values ($E_{JT} = 30–80$ cm^{-1}),[80–83] and together with the values of the vibronic coupling constants, confirm the dynamic character of the JT effect.

In VCl_4, for the first time, some interesting features related to the DFT scheme for the calculation of the JT parameters were observed.[58] These observations are found to be general in other cases. The first one is related to the energies of different electron distributions in step 2 (Fig. 4), which should be equal for all the possibilities. However, in practice, this is not the case due to the nature of the exchange-correlation functional involved in practical DFT calculations. The second finding is that ordering of orbitals in step 2 is *non-aufbau*. In other words, the singly occupied MO stays, after the energy minimization, above the lowest empty orbital. The expected orbital ordering is usually restored after relaxation of the geometry (step 3). When distortion is very small, *e.g.*, in VCl_4, the occupation stays even after the geometry optimization in step 3. It should be pointed out that the JT effect is a change in geometry due to a lowering of the total energy and the KS MO energies do not need to reflect that. In DFT, the total energy is not equal to the sum of the KS orbital energies. The third remark is that partial occupation of degenerate orbitals (step 1) usually leads to lower energy than the one-electron-one-orbital occupancy (step 2), because of different self-interaction errors in the two cases. In the case of VCl_4, the energy from step 1 can be even lower than the final energies from step 3, giving a misleading result.

The cyclopentadienyl radical ($^\bullet C_5H_5$) is one of the most studied molecules from the JT perspective, and the theoretical methods employed range from simple MO calculations[102] to high-level *ab-initio* calculations (Table II). Studies of Mueller *et al.* who used complete active space methods ($E_{JT} = 2147$ cm^{-1})[86] and dispersed fluorescence spectroscopy ($E_{JT} = 1237$ cm^{-1}),[86] as well as fitting *ab-initio* calculations to the spectra ($E_{JT} = 1463$ cm^{-1})[86] are considered to be

benchmark results for the determination of the JT parameters in the cyclopentadienyl radical. The authors also identified three dominant normal modes necessary to explain their results. Results obtained by DFT are comparable,[37,66] or in some cases even better than other theoretical methods (Table II). With the IDP model, it was possible to identify the three most important vibrations (C–C stretch, C–C–C bending, and C–C–H bending),[66] in agreement with the computational and experimental studies by Miller *et al.*[86]

TABLE II. Summary of various computational methods used to study the JT effect in the cyclopentadienyl radical

Method[a]	E_{JT} / cm^{-1}	Reference
MO	560	Liehr 1956[102]
MO	728	Snyder 1960[103]
MO	495	Hobey *et al.* 1960[104]
HF/STO-3G	5072	Meyer *et al.* 1979[105]
CI/STO-3G	2484	Borden 1979[106]
HF/6-311+G*	1452	Cuhna *et al.* 1999[107]
MP2/6-311+G*	3065	Cuhna *et al.* 1999[107]
MP4/6-311+G*	2581	Cuhna *et al.* 1999[107]
CCSD/6-311+G*	1613	Cuhna *et al.* 1999[107]
CCSD(T)/6-311+G*	1613	Cuhna *et al.* 1999[107]
CASSCF/cc-PVDZ	2139	Bearpark *et al.* 1999[108]
CASSCF/6-31G*	2147	Miller *et al.*, 2001[86]
CASSCF/6-31G*	1463	Miller *et al.*, 2001[86]
CASSCF/cc-PVDZ	1665	Kiefer *et al.* 2001[109]
CISD/cc-PVDZ	2553	Zilberg *et al.* 2002[110]
EOMIP-CCSD/DZP	1581	Stanton *et al.* 2008[111]
DFT(LDA)/TZP	1253	Zlatar *et al.*, 2009[37]
DFT (B3LYP)/TZP	1685	Zlatar *et al.*, 2013[73]
IDP	1239	Zlatar *et al.*, 2010
Exp.	1237	Miller *et al.*, 2001[86]

[a]HF – Hartree–Fock; CI – configuration Interaction; MPN – Moeller–Plesset perturbation theory of order N; CCSD(T) – coupled cluster single, double (triple) excitations; CASSCF – complete-active-space SCF; CISD – single and double excitations, single reference CI method; EOMIP-CCSD – equation-of-motion ionization potential coupled cluster single, double excitations; LDA – local density approximation; B3LYP – Becke's 3-parameters Lee–Yang–Parr hybrid functional

DFT results show that the energy difference between the two distorted LS structures of the cyclopentadienyl radical is only around 1.5 cm^{-1}.[37,66] Hence, it is an example of a dynamic JT effect. According to DFT calculations, the $^2A_2$ structure (en-allyl) is a transition state, while $^2B_1$ (dienyl) is a minimum.[37,66] This is in agreement with CASSCF(5,5)/cc-pVTZ[112] and CASSCF(5,5)/6-31G*[86] calculations that report the dienyl structure to be a minimum and Δ to be 4.5 and 3.6 cm^{-1}, respectively. The conversion between the $^2A_2$ and $^2B_1$ states goes around the JT cusp, Fig. 6. Due to the five-fold permutational symmetry of the cyclopentadienyl radical, there needs to be five equivalent dienyl and five equi-

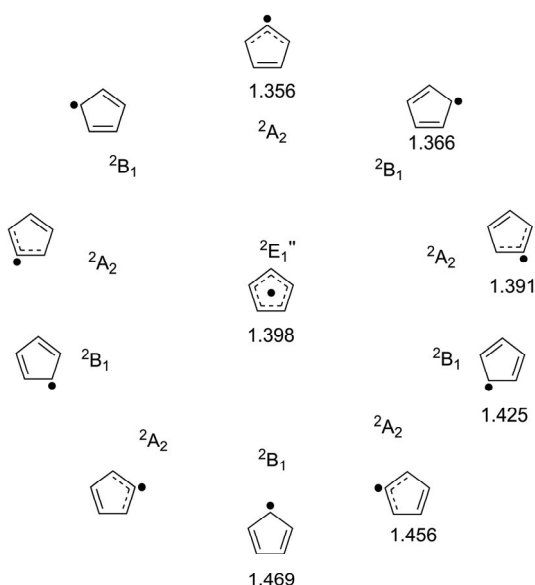valent en-alyl structures,[113] which interconvert to each other with practically no energy barrier.

Fig. 6. Schematic representation of the pseudorotation on the lowest sheet of the adiabatic potential energy surface of the cyclopentadienyl radical. C–C bond length, Å, which is chosen to be the linear transit parameter is marked.

According to DFT calculations, the $^2A_2$ conformations have one imaginary frequency belonging to the B_2 irrep in C_{2v} point group, which lowers the symmetry to C_s. Pseudorotation of the cyclopentadienyl radical goes along the path that has C_s symmetry, except at the ten configurations of C_{2v} symmetry that correspond to the stationary points on the potential energy surface. To test whether such a small Δ is just due to the numerical noise in DFT calculations, the lowest sheet of the adiabatic potential energy surface was explored using relaxed linear transit calculations. The results are shown in Fig. 7. One of the C–C bond lengths was varied from 1.469 Å, *i.e.*, single C–C bond in $^2B_1$, to 1.336 Å, *i.e.*, double C=C bond in $^2A_2$. The symmetry was constrained to C_s. All the remaining coordinates were allowed to be optimized. This process corresponds to half the pseudorotation depicted in Fig. 6.

In addition to the cyclopentadienyl radical, the JT effect in the family of cyclic conjugated hydrocarbons was analyzed,[66] including the benzene cation ($C_6H_6^+$), the benzene anion ($C_6H_6^-$) and the tropyl radical ($^•C_7H_7$). All three molecules have a double degenerate electronic ground state ($^2E_{1g}$, $^2E_{1g}$ and E_2'', respectively) in the HS configuration (D_{6h}, D_{6h} and D_{7h}, respectively) that is coupled with double degenerate JT active normal modes (e_{1g}, e_{1g} and e_3', respectively). The DFT results are in excellent agreement with previous studies (Table I). The IDP model showed that the C–C stretch is most important for energy stabilization, while C–C–C bend, and C–C–H bend contribute more to the

R_{JT}. The energy component analysis along IDP revealed two distinct regions. Most of the energy stabilization is achieved by electron–nuclear attractions in the first region, where the C–C stretch prevails. Other forces due to electron–electron, nuclear–nuclear, and kinetic interactions are dominant in the second region. In the second region, little stabilization is achieved, and the molecules relax toward the LS stationary point *via* bending deformations.
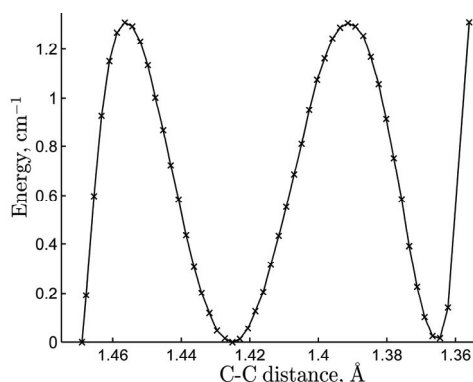

Fig. 7. Linear transit calculations used for the exploration of the lowest sheet of the potential energy surface of the cyclopentadienyl radical.

In the benzene cation and anion, the symmetry of the HS nuclear configuration, the symmetry of the ground electronic state, and symmetry of the JT active vibrations are all the same. However, the minimum on the potential energy surface is different. While in $C_6H_6^+$ the minimum is D_{2h} conformation, in $C_6H_6^-$ due to pseudo-Jahn–Teller coupling of the ground $\pi*$ electronic state with the excited $\sigma*$ state, the C_{2v} conformation is found to be the global minimum. The out-of-plane C_{2v} geometry obtained is a consequence of both JT and pseudo-JT distortion.

Corannulene ($C_{20}H_{10}$) and coronene ($C_{24}H_{12}$) and their ions are interesting molecules because besides being building blocks for fullerene, they also have application in electronic devices. Distortion in these molecules,[68] as in other carbohydrates always starts with the modes that are predominantly C–C stretching, and these modes contribute the most to the overall distortion due to the descent in symmetry.

The neutral fullerene C_{60} molecule has very high symmetry. It belongs to the I_h point group, with a high degree of degeneracies. The highest occupied molecular orbital is fivefold degenerate (h_u), and the lowest unoccupied molecular orbital is triply degenerate (t_{1u}), Fig. 8. The distortion in the JT active C_{60}^+ and C_{60}^- may lead to the structures belonging to the three different epikernel subgroups, *i.e.*, to the structures with D_{5d}, D_{3d} or D_{2h} symmetry. The JT active modes in C_{60}^- belong to H_g irrep. The stable geometry of the C_{2h} symmetry, resulting from JT distortions of double degenerate states in D_{5d} or D_{3d}, is predicted to be the most stable.[92] In C_{60}^-, the energy differences between different

ZLATAR and GRUDEN

distorted structures are very small.[92] According to DFT calculations, the $^2A_{1u}$ conformation in the D_{5d} point group is the global minimum for C_{60}^+.[77] The vibronic coupling in C_{60}^+ is very complicated. The D_{5d} structure is a consequence of the h_g modes described by one set of the linear vibronic coupling coefficients. D_{3d} structures are due to the distortion led by the h_g modes with a different set of vibronic coupling coefficients, but g_g modes are also active. In addition, the totally symmetric normal modes also have non-zero vibronic coupling. Utilizing the IDP model, all the vibronic coupling constants of all normal modes in C_{60}^+ were calculated[77] – two a_g, six g_g and two sets of constants for eight h_g modes. The obtained values agree with previously calculated vibronic coupling constants from the gradient of the HOMO level.[91] The vibronic coupling constants of the eight h_g modes and two ag modes in C_{60}^- were also calculated[92] by the IDP model, which agreed with previous reports.[91,114] The choice of the geometry of the I_h structure was also highlighted, in particular, related to the contributions of totally symmetric normal modes. According to IDP, most of the stabilization energy is achieved close to the I_h point by the hardest JT active modes. These modes have a large C–C stretch character. The relaxation of the geometry in the final part of the distortion path is encountered by softer modes. The situation is completely analog to the JT effect in the cyclopentadienyl radical and the benzene cation.
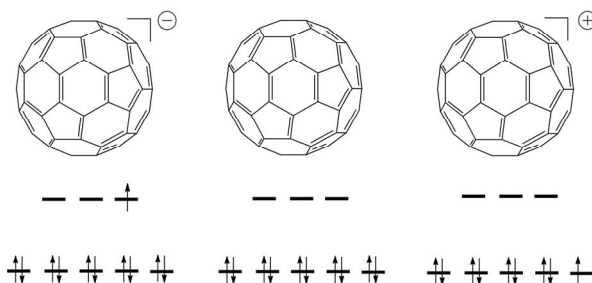

Fig. 8. Qualitative MO scheme of the fullerene anion, neutral fullerene, and the fullerene cation.

JT instable metallocenes, *e.g.*, low spin d^7 cobaltocene ($CoCp_2$, $Cp = C_5H_5$), low spin d^5 manganocene ($MnCp_2$) and low spin ferrocenyl cation, ($[FeCp_2]^+$) are typical examples of multimode JT distortions. The HS conformation of metallocenes can be either D_{5h} if the two cyclopentadienyl rings are eclipsed, or D_{5d} if two rings are staggered. According to DFT calculations, the eclipsed conformation is the more stable one,[72] and descent in symmetry due to the distortion goes to C_{2v} LS structures. The E_{JT} agrees with the experimental results, and do not differ much for the three metallocenes (Table I).[80,95] In the C_{2v} minimum energy conformation, both cobaltocene and manganocene have 16 totally symmetrical normal modes that all could in principle contribute to the distortion.

With IDP model, not only their contribution to the R_{JT}, but also their contribution to the E_{JT} was determined.[67]

The ground state of cobaltocene is $^2E_1''$ with a single electron in e_1'' MO. This MO is antibonding between metal d_{xz} (or d_{yz}) and the ligand π-system. Using group theory, it is easy to show that the distortion coordinate is e_2'. Out of 16 vibrations, 4 contribute more than 95 % to the E_{JT}, and all four are first order JT active, *i.e.*, e_2', and all are located on cyclopentadienyl ring, which is no longer planar. Although in most cases the electronic distortion due to the JT effect is mainly localized on the central metal ion, here it is delocalized over the ligands. The symmetry of the electronic ground state in the HS point pushed the distortion towards perturbation of the aromaticity of the Cp rings. In other words, JT induces conformational changes of the ligands, and out-of-plane ring distortion and C–H wagging minimize the antibonding interaction between the single occupied d orbital of the Co(II) ion and the π system of the Cp rings.

Manganocene with 5 electrons in d-orbitals is in the $^2E_2'$ ground state (low spin is the most stable one) with a single hole in the nonbonding e_2' orbital in the D_{5h} symmetry, with the very close lying $^2A_1'$ state. Distortion lowers the symmetry to C_{2v} along the e_1' normal coordinates. Skeletal vibrations contribute the most to the E_{JT} and enhance small bonding interactions between the d-orbitals and the π-system of Cp rings.[67] These distortions are localized around the metal. However, IDP analysis revealed that there is one more vibrational mode that bends the two Cp rings and has an influence on the JT distortion, but does not bring a dominant energetic contribution.[67,96]

Another intriguing feature is the unusual behavior of manganocene compared to its isoelectronic analog ferrocenium cation and other metallocenes. Namely, in the solid state, manganocene forms a zig-zag polymer in which the ground state is the high spin state, which was not observed in any other case.[115] Our thorough study in which DFT, energy decomposition analysis and IDP methods were applied, revealed the reason behind this peculiar behavior of MnCp$_2$.[96] It was shown that the close lying $^6A_1'$ state allows conversion to the HS state present in the zigzag polymer. Moreover, the close lying excited state $^2A_1'$ enables ligand deformation through pseudo-JT coupling and triggers the polymerization. Hence, the unique behavior of manganocene has been rationalized and explained by its degenerate ground state and close lying electronic and spin states.[96]

Phthalocyanine trianion (Pc^{3-}), magnesium phthalocyanine ion (MgPc$^-$) and manganese phthalocyanine (MnPc) are all prone to JT distortion. Detailed analysis[71] showed that the coordinated metal dictated the way of breaking the symmetry: while in MgPc$^-$, the distortion is mainly localized on the ligand, in MnPc, central metal ion presents the trigger for the occurrence of JT distortion over the whole system. This difference was rationalized with IDP analysis that indicated

different normal modes responsible for the JT effect in these similar systems. The linear vibronic coupling constants of all 24 JT active modes were determined by IDP model that agreed with previous work.[71]

A study[98] on complexes of bis(1,4,7-triazacyclononane) (TACN) with some first-row transition metal ions with the ground term subject to JT distortion, revealed that vibronic coupling must be taken into consideration, even when the JT distortion is negligible because it can contribute to all the properties of the system. In all cases, the E_{JT} values obtained by DFT calculations were in excellent agreement with experimentally observed ones, confirming the excellent ability of the DFT approach to calculate JT parameters even when the complicated electronic structure of transition metal compounds have to be considered. Furthermore, IDP analysis gave further insight into what is happening during the distortion and distinguished the most important normal modes out of 71 to the E_{JT} and R_{JT}. It has been shown that the second coordination sphere does not influence the values of the JT parameters,[98] as in the case of $[Cu(en)_3]^{2+}$ (en is ethylenediamine) and $[Cu(eg)_3]^{2+}$ (eg is ethylene glycol).[75]

$Pt(PF_3)_4$ is tetrahedral d^0 molecule in the $^1A_1$ ground electronic state. This molecule is an important precursor for focused electron beam induced processing.[116] In this technique, a focused beam of electrons is used to initiate the dissociation of ligands in the precursor, ideally resulting in a pure metal deposit. Several processes occur during this process, and the importance of so-called neutral dissociation was first highlighted in $Pt(PF_3)_4$.[117] Neutral dissociation is the dissociation of electronically excited states initiated by incoming electrons. At first sight, this small symmetric molecule is not related to the JT effect. However, its lowest excited states are degenerate (lowest $^{1,3}T_1$ and $^{1,3}T_2$) and are consequently subject to JT distortion. Distortion in these excited states is asymmetric Pt–P stretch of T_2 symmetry and this is exactly the dissociation coordinate. Therefore, the JT effect in the excited states triggers dissociation.[117] These four excited states are directly dissociative, while other excited states are dissociative *via* many conical intersections.[117]

Five-coordinated Ni(II) trigonal–bipyramidal complexes (D_{3h}) in a high spin are in $^3E'$ ground state, hence prone to the JT distortion to the C_{2v} structure. It has been shown that controlling the geometry of a transition metal complex is the way to chemically control their magnetic properties, particularly that spin–orbit coupling (SOC) could be used to tune the magnetic anisotropy.[18,19] If the SOC is higher, the magnetic anisotropy has a greater value. Knowing the fact that both coordination of the ligands and the partial quenching of the SOC due to JT distortions reduce the magnetic anisotropy from its ideal, the free ion value, the system ($[NiCl_3(Hdabco)_2]^+$, dabco is 1,4-diazabicyclo[2.2.2]-octane), was found in which the bulky dabco axial ligands prevent distortion.[18] As a consequence of quenched JT, the calculations revealed,[18] and later it was experimentally con-

firmed,[118] that this complex displays the largest magnetic anisotropy ever observed for a mononuclear Ni(II) complex.

4. CONCLUSIONS

Cast in the form of authors' review paper, this work summarizes the results obtained by a special procedure within the framework of DFT, for the analysis of the JT effect in many different molecules. The theoretical background and practical computational recipe of this non-empirical and effective method are given. Treatment of the multimode JT problem with the IDP approach provides microscopic insight into the symmetry breaking process and rationalize many manifestations of vibronic coupling. Therefore, the fast and reliable method presented herein could be considered as the preferable tool for the investigation of adiabatic potential energy surface of the JT active molecules.

И З В О Д

ИЗРАЧУНАВАЊЕ ЈАН–ТЕЛЕРОВИХ ПАРАМЕТАРА ПРИМЕНОМ ТЕОРИЈЕ ФУНКЦИОНАЛА ГУСТИНЕ

МАТИЈА ЗЛАТАР[1] и МАЈА ГРУДЕН[2]

[1]Универзишеш у Беоīраду-Инсшишуш за хемију, шехнолоīију и мешалурīију, Ценшар за хемију, Њеīошева 12, Беоīрад и [1]Универзишеш у Беоīраду-Хемијски факулшеш, Сшуденшски шрī 12–16, Беоīрад

У овом прегледном раду, представљена је не-емпиријска процедура за израчунавање Јан–Телерових параметара применом теорије функционала густине, која не зависи од конкретног система који се проучава. Представљен је и модел својственог пута дисторзије, који даје додатни увид у механизам дисторзије. Сумирани резултати и њихово поређење са експериментално процењеним вредностима, као и поређење са резултатима *ab initio* прорачуна високог нивоа, доказују тачност и велику применљивост коришћене процедуре. Такође, овде приказани рачунарски приступ даје много одговоре на интригантне особине Јан–Телер-активних молекула.

(Примљено 10. маја, прихваћено 25. јуна 2019)

REFERENCES

1. H. A. Jahn, E. Teller, *Proc. R. Soc., A* **161** (1937) 220 (https://dx.doi.org/10.1098/rspa.1937.0142)
2. O. Kahn, *Structure électronique des éléments de transition: ions et molécules complexes*, Presses universitaires de France, 1977
3. J. G. Bednorz, K. A. Müler, *Perovskite-Type Oxides – The New Approach to High-Tc Superconductivity - Nobel Lecture*, in *Nobel Lect. Phys. 1981–1990*, G. Ekspang, Ed., World Scientific Publishing Co, Singapore, 1993, pp. 424–457
4. I. B. Bersuker, *The Jahn–Teller Effect*, Cambridge University Press, Cambridge, 2006 (https://dx.doi.org/10.1017/CBO9780511524769)
5. R. Renner, *Z. Physik* **92** (1934) 172 (https://dx.doi.org/10.1007/BF01350054)
6. U. Öpik, M. H. L. Pryce, *Proc. R. Soc., A* **238** (1957) 425 (https://dx.doi.org/10.1098/rspa.1957.0010)

7. I. B. Bersuker, *Chem. Rev.* **113** (2013) 1351 (https://dx.doi.org/10.1021/cr300279n)
8. T. Azumi, K. Matsuzaki, *Photochem. Photobiol.* **25** (1977) 315 (https://dx.doi.org/10.1021/cr300279n)
9. H. Köppel, W. Domcke, L. S. Cederbaum, *Multimode Molecular Dynamics Beyond the Born–Oppenheimer Approximation*, Adv. Chem. Physics, Vol. 57, in I. Prigogine, S. A. Rice, Eds., Wiley 2007, pp. 59–246 (https://dx.doi.org/10.1002/9780470142813.ch2)
10. A. J. Millis, P. B. Littlewood, B. I. Shraiman, *Phys. Rev. Lett.* **74** (1995) 5144 (https://dx.doi.org/10.1103/PhysRevLett.74.5144)
11. A. J. Millis, B. I. Shraiman, R. Mueller, *Phys. Rev. Lett.* **77** (1996) 175 (https://dx.doi.org/10.1103/PhysRevLett.77.175)
12. J. G. Bednorz, K. A. Müller, *Z. Physik, B: Cond. Matter* **64** (1986) 189 (https://dx.doi.org/10.1007/BF01303701)
13. R. H. Zadik, Y. Takabayashi, G. Klupp, R. H. Colman, A. Y. Ganin, A. Potočnik, P. Jeglič, D. Arčon, P. Matus, K. Kamarás, Y. Kasahara, Y. Iwasa, A. N. Fitch, Y. Ohishi, G. Garbarino, K. Kato, M. J. Rosseinsky, K. Prassides, *Sci. Adv.* **1** (2015) e1500059 (https://dx.doi.org/10.1126/sciadv.1500059)
14. M. G. Schultz, T. S. Nunner, F. von Oppen, *Phys. Rev., B* **77** (2008) 075323 (https://dx.doi.org/10.1103/PhysRevB.77.075323)
15. I. B. Bersuker, *Phys. Lett.* **20** (1966) 589 (https://dx.doi.org/10.1016/0031-9163(66)91127-9)
16. P. Garcia-Fernandez, I. B. Bersuker, *Phys. Rev. Lett.* **106** (2011) 246406 (https://dx.doi.org/10.1103/PhysRevLett.106.246406)
17. M. Atanasov, J. M. Zadrozny, J. R. Long, F. Neese, *Chem. Sci.* **4** (2013) 139 (https://dx.doi.org/10.1039/c2sc21394j)
18. M. Gruden-Pavlović, M. Perić, M. Zlatar, P. Garcia-Fernandez, *Chem. Sci.* **5** (2014) 1453 (https://dx.doi.org/10.1039/C3SC52984C)
19. M. Perić, A. García-Fuente, M. Zlatar, C. Daul, S. Stepanović, P. García-Fernández, M. Gruden-Pavlović, *Chem. Eur. J.* **21** (2015) 3716 (https://dx.doi.org/10.1002/chem.201405480)
20. W. Domcke, H. Köppel, L. S. Cederbaum, *Mol. Phys.* **43** (1981) 851 (https://dx.doi.org/10.1080/00268978100101721)
21. M. Perić, S. D. Peyerimhoff, *J. Mol. Spectrosc.* **212** (2002) 153 (https://dx.doi.org/10.1006/JMSP.2002.8534)
22. M. Perić, S. D. Peyerimhoff, *J. Chem. Phys.* **102** (1995) 3685 (https://dx.doi.org/10.1063/1.468599)
23. M. Mitić, R. Ranković, M. Milovanović, S. Jerosimić, M. Perić, *Chem. Phys.* **464** (2016) 55 (https://dx.doi.org/10.1016/J.CHEMPHYS.2015.11.002)
24. M. Perić, *Mol. Phys.* **105** (2007) 59 (https://dx.doi.org/10.1080/00268970601129076)
25. M. Perić, B. Ostojić, J. Radić-Perić, *Phys. Rep.* **290** (1997) 283 (https://dx.doi.org/10.1016/S0370-1573(97)00018-5)
26. M. Perić, S. D. Peyerimhoff, R. J. Buenker, *Mol. Phys.* **49** (1983) 379 (https://dx.doi.org/10.1080/00268978300101241)
27. I. B. Bersuker, *Spontaneous Symmetry Breaking in Matter Induced by Degeneracies and Pseudodegeneracies*, in Adv. Chem. Physics, Vol. 160, S. A. Rice, A. R. Dinner, Eds., Wiley, 2016, pp. 159–208 (https://dx.doi.org/10.1002/9781119165156.ch3)
28. P. Garcia-Fernandez, I. B. Bersuker, *Int. J. Quantum Chem.* **112** (2012) 3025 (https://dx.doi.org/10.1002/qua.24204)

29. P. García-Fernández, J. A. Aramburu, M. Moreno, M. Zlatar, M. Gruden-Pavlovic, *J. Chem. Theory Comput.* (2014) 1824 (https://dx.doi.org/10.1021/ct4011097)
30. Y. Liu, I. B. Bersuker, P. Garcia-Fernandez, J. E. Boggs, *J. Phys. Chem., A* **116** (2012) 7564 (https://dx.doi.org/10.1021/jp3032836)
31. P. Garcia-Fernandez, J. A. Aramburu, M. Moreno, *Phys. Rev., B* **83** (2011) 174406 (https://dx.doi.org/10.1103/PhysRevB.83.174406)
32. R. F. W. Bader, *Mol. Phys.* **3** (1960) 137 (https://dx.doi.org/10.1103/10.1080/00268976000100161)
33. R. F. W. Bader, *Can. J. Chem.* **40** (1962) 1164 (https://dx.doi.org/10.1139/v62-178)
34. R. F. W. Bader, A. D. Bandrauk, *J. Chem. Phys.* **49** (1968) 1666 (https://dx.doi.org/10.1063/1.1670293)
35. R. G. Pearson, *J. Am. Chem. Soc.* **91** (1969) 4947 (https://dx.doi.org/10.1021/ja01046a001)
36. R. G. Pearson, *Symmetry Rules for Chemical reactions*, A Wiley-Interscience Publication, New York,1976 (https://dx.doi.org/10.1002/bbpc.19790830620)
37. M. Zlatar, C.-W. Schläpfer, C. Daul, *A New Method to Describe Multimode Jahn–Teller Efect Using Density Functional Theory*, in *The Jahn–Teller-Effect Fundamentals and Implications for Physics and Chemistry*, H. Koeppel, D. R. Yarkoni, H. Barentzen, Eds., Springer Series in Chemical Physics, Vol. 97, 2009, pp. 131 (https://dx.doi.org/10.1007/978-3-642-03432-9_6)
38. A. R. Ilkhani, N. N. Gorinchoy, I. B. Bersuker, *Chem. Phys.* **460** (2015) 106 (https://dx.doi.org/10.1016/J.CHEMPHYS.2015.07.015)
39. A. R. Ilkhani, W. Hermoso, I. B. Bersuker, *Chem. Phys.* **460** (2015) 75 (https://dx.doi.org/10.1016/J.CHEMPHYS.2015.02.017)
40. P. Garcia-Fernandez, I. B. Bersuker, J. A. Aramburu, M. T. Barriuso, M. Moreno, *Phys. Rev., B* **71** (2005) 184110 (https://dx.doi.org/10.1103/PhysRevB.71.184117)
41. Y. Liu, I. B. Bersuker, W. Zou, J. E. Boggs, *J. Chem. Theory Comput.* **5** (2009) 2679 (https://dx.doi.org/10.1021/ct9002515)
42. R. G. Parr, W. Yang, *Density-Functional Theory of Atoms and Molecules*, Oxford University Press, Oxford, 1989 (https://global.oup.com/academic/product/density-functional-theory-of-atoms-and-molecules-9780195092769?cc=rs&lang=en&)
43. C. J. Cramer, D. G. Truhlar, *Phys. Chem. Chem. Phys.* **11** (2009) 10757 (https://dx.doi.org/10.1039/b907148b)
44. F. Neese, *Coord. Chem. Rev.* **253** (2009) 526 (https://dx.doi.org/10.1016/j.ccr.2008.05.014)
45. J. P. Perdew, A. Ruzsinszky, *Int. J. Quantum Chem.* **110** (2010) 2801 (https://dx.doi.org/10.1002/qua.22829)
46. K. Burke, L. O. Wagner, *Int. J. Quantum Chem.* **113** (2013) 96 (https://dx.doi.org/10.1002/qua.24259)
47. A. D. Becke, *J. Chem. Phys.* **140** (2014) 18A301 (https://dx.doi.org/10.1063/1.4869598)
48. H. S. Yu, S. L. Li, D. G. Truhlar, *J. Chem. Phys.* **145** (2016) 130901 (https://dx.doi.org/10.1063/1.4963168)
49. P. Hohenberg, W. Kohn, *Phys. Rev.* **136** (1964) B864 (https://dx.doi.org/10.1103/PhysRev.136.B864)
50. L. Goerigk, A. Hansen, C. Bauer, S. Ehrlich, A. Najibi, S. Grimme, *Phys. Chem. Chem. Phys.* **19** (2017) 32184 (https://dx.doi.org/10.1039/C7CP04913G)

51. I. B. I. B. Bersuker, *J. Comp. Chem.* **18** (1997) 260 (https://dx.doi.org/10.1002/(SICI)1096-987X(19970130)18:2<260::AID-JCC10>3.0.CO;2-M)
52. I. G. G. Kaplan, *J. Mol. Struct.* **838** (2007) 39 (https://dx.doi.org/10.1016/J.MOLSTRUC.2007.01.012)
53. I. B. Bersuker, *J. Phys. Conf. Ser.* **833** (2017) 012001 (https://dx.doi.org/10.1088/1742-6596/833/1/012001)
54. M. Levy, *Phys. Rev., A* **26** (1982) 1200 (https://dx.doi.org/10.1103/PhysRevA.26.1200)
55. M. Levy, *Int. J. Quantum Chem.* **110** (2010) 3140 (https://dx.doi.org/10.1002/qua.22895)
56. A. K. Theophilou, *J. Phys., C: Solid State Phys.* **12** (1979) 5419 (https://dx.doi.org/10.1088/0022-3719/12/24/013)
57. A. K. Theophilou, P. G. Papaconstantinou, *Phys. Rev., A* **61** (2000) 022502 (https://dx.doi.org/10.1103/PhysRevA.61.022502)
58. M. Filatov, *J. Chem. Theory Comput.* **9** (2013) 4526 (https://dx.doi.org/10.1021/ct400598b)
59. R. Requist, E. K. U. Gross, *Phys. Rev. Lett.* **117** (2016) 193001 (https://dx.doi.org/10.1103/PhysRevLett.117.193001)
60. R. Baer, *Phys. Rev. Lett.* **104** (2010) 073001 (https://dx.doi.org/10.1103/PhysRevLett.104.073001)
61. J. M. García-Lastra, M. T. Barriuso, J. A. Aramburu, M. Moreno, *Chem. Phys.* **317** (2005) 103 (https://dx.doi.org/10.1016/j.chemphys.2005.06.004)
62. W. L. Clinton, B. Rice, *J. Chem. Phys.* **30** (1959) 542 (https://dx.doi.org/10.1063/1.1729984)
63. H. Nakatsuji, *J. Am. Chem. Soc.* **96** (1974) 30 (https://dx.doi.org/10.1021/ja00808a005)
64. R. Bruyndonckx, C. Daul, P. T. Manoharan, E. Deiss, R. Bruyndockx, C. Daul, P. T. Manoharan, E. Deiss, *Inorg. Chem.* **36** (1997) 4251 (https://dx.doi.org/10.1021/ic961220+)
65. T. K. Kundu, R. Bruyndonckx, C. Daul, P. T. Manoharan, *Inorg. Chem.* **38** (1999) 3931 (https://dx.doi.org/10.1021/ic981111q)
66. M. Gruden-Pavlović, P. García-Fernández, L. Andjelković, C. Daul, M. Zlatar, *J. Phys. Chem., A* **115** (2011) 10801 (https://dx.doi.org/10.1021/jp206083j)
67. M. Zlatar, M. Gruden-Pavlović, C. W. Schläpfer, C. Daul, *J. Mol. Struct. THEOCHEM* **954** (2010) 86 (https://dx.doi.org/10.1016/j.theochem.2010.04.020)
68. L. Andjelković, M. Gruden-Pavlović, M. Zlatar, *Chem. Phys.* **460** (2015) 64 (https://dx.doi.org/10.1016/j.chemphys.2015.05.007)
69. M. Zlatar, M. Gruden-Pavlović, C.-W. Schläpfer, C. Daul, *Chimia* **64** (2010) 161 (https://dx.doi.org/10.2533/chimia.2010.161)
70. M. Perić, L. Andjelković, M. Zlatar, C. Daul, M. Gruden-Pavlović, *Polyhedron* **80** (2014) 69 (https://dx.doi.org/10.1016/j.poly.2014.02.005)
71. L. Andjelkovic, S. Stepanovic, F. Vlahovic, M. Zlatar, M. Gruden, L. Andjelković, S. Stepanović, F. Vlahović, M. Zlatar, M. Gruden, *Phys. Chem. Chem. Phys.* **18** (2016) 29122 (https://dx.doi.org/10.1039/C6CP03859J)
72. M. Zlatar, C.-W. Schläpfer, E. P. Fowe, C. Daul, *Pure Appl. Chem.* **81** (2009) 1397 (https://dx.doi.org/10.1351/PAC-CON-08-06-04)
73. L. Andjelković, M. Gruden-Pavlović, C. Daul, M. Zlatar, *Int. J. Quantum Chem.* **113** (2013) 859 (https://dx.doi.org/10.1002/qua.24245)
74. M. Atanasov, P. Comba, C. a Daul, A. Hauser, *J. Phys. Chem., A* **111** (2007) 9145 (https://dx.doi.org/10.1021/jp0731912)

75. M. Gruden-Pavlović, M. Zlatar, C.-W. Schläpfer, C. Daul, *J. Mol. Struct. THEOCHEM* **954** (2010) 80 (https://dx.doi.org/10.1016/j.theochem.2010.03.031)
76. M. Swart, M. Gruden, *Acc. Chem. Res.* **49** (2016) 2690 (https://dx.doi.org/10.1021/acs.accounts.6b00271)
77. H. Ramanantoanina, M. Zlatar, P. García-Fernández, C. Daul, M. Gruden-Pavlović, *Phys. Chem. Chem. Phys.* **15** (2013) 1252 (https://dx.doi.org/10.1039/c2cp43591h)
78. V. P. Khlopin, V. Z. Polinger, I. B. Bersuker, *Theor. Chim. Acta* **48** (1978) 87 (https://dx.doi.org/10.1007/BF02399020)
79. I. B. Bersuker, V. Z. Polinger, *Vibronic interactions in Molecules and Crystals*, Springer--Verlag, Berlin, 1989 (https://www.springer.com/gp/book/9783642834813)
80. J. H. Ammeter, L. Zoller, J. Bachmann, P. Baltzer, E. Gamp, R. Bucher, E. Deiss, *Helv. Chim. Acta* **64** (1981) 1063 (https://dx.doi.org/10.1002/chin.198141061)
81. F. A. Blankenship, R. L. Belford, *J. Chem. Phys.* **36** (1962) 633 (https://dx.doi.org/10.1063/1.1732585)
82. R. B. Johannesen, G. A. Candela, T. Tsang, *J. Chem. Phys.* **48** (1968) 5544 (https://doi.org/10.1063/1.1668254)
83. Y. Morino, H. Uehara, *J. Chem. Phys.* **45** (1966) 4543 (https://dx.doi.org/10.1063/1.1727535)
84. H. von Busch, V. Dev, H.-A. Eckel, S. Kasahara, J. Wang, W. Demtröder, P. Sebald, W. Meyer, *Phys. Rev. Lett.* **81** (1998) 4584 (https://dx.doi.org/10.1103/PhysRevLett.81.4584)
85. J. Gaus, K. Kobe, V. Bonacic-Koutecky, H. Kuehling, J. Manz, B. Reischl, S. Rutz, E. Schreiber, L. Woeste, *J. Phys. Chem.* **97** (1993) 12509 (https://dx.doi.org/10.1021/j100150a011)
86. B. E. Applegate, T. A. Miller, *J. Chem. Phys.* **114** (2001) 4855 (https://dx.doi.org/10.1063/1.1348275)
87. B. E. Applegate, T. A. Miller, *J. Chem. Phys.* **117** (2002) 10654 (https://dx.doi.org/10.1063/1.1520531)
88. V. Perebeinos, P. B. Allen, M. Pederson, *Phys. Rev., A* **72** (2005) 12501 (https://dx.doi.org/10.1103/PhysRevA.72.012501)
89. K. Tokunaga, T. Sato, K. Tanaka, *J. Chem. Phys.* **124** (2006) 154303 (https://dx.doi.org/10.1063/1.2184317)
90. I. Sioutis, V. L. Stakhursky, G. Tarczay, T. A. Miller, *J. Chem. Phys.* **128** (2008) 084311 (https://dx.doi.org/10.1063/1.2829471)
91. N. Manini, A. Dal Corso, M. Fabrizio, E. Tosatti, *Philos. Mag., B* **81** (2001) 793 (https://dx.doi.org/10.1080/13642810110062663)
92. H. Ramanantoanina, M. Gruden-Pavlovic, M. Zlatar, C. Daul, *Int. J. Quantum Chem.* **113** (2013) 802 (https://dx.doi.org/10.1002/qua.24080)
93. T. Yamabe, K. Yahara, T. Kato, K. Yoshizawa, *J. Phys. Chem., A* **104** (2000) 589 (https://dx.doi.org/10.1021/jp992496g)
94. T. Kato, K. Yoshizawa, *J. Chem. Phys.* **110** (1999) 249 (https://dx.doi.org/10.1063/1.478100)
95. R. Bucher, *ESR-Untersuchungen an Jahn-Teller-Aktiven Sandwitchkomplexen*, ETH Zuerich, 1977 (https://dx.doi.org/10.3929/ethz-a-000150322)
96. S. Stepanović, M. Zlatar, M. Swart, M. Gruden, *J. Chem. Inf. Model.* **59** (2019) 1806 (https://doi.org/10.1021/acs.jcim.8b00870)
97. J. Tóbik, E. Tosatti, *J. Mol. Struct.* **838** (2007) 112 (https://doi.org/10.1016/J.MOLSTRUC.2006.12.051)

98. M. Zlatar, M. Gruden-Pavlovic, M. Guell, M. Swart, M. Gruden-Pavlović, M. Güell, M. Swart, *Phys. Chem. Chem. Phys.* **15** (2013) 6631 (https://dx.doi.org/10.1039/C2CP43735J)

99. P. Chaudhuri, K. Oder, K. Wieghardt, J. Weiss, J. Reedijk, W. Hinrichs, J. Wood, A. Ozarowski, H. Stratemaier, D. Reinen, *Inorg. Chem.* **25** (1986) 2951 (https://dx.doi.org/10.1021/ic00237a007)

100. K. Wieghardt, W. Walz, B. Nuber, J. Weiss, A. Ozarowski, H. Stratemeier, D. Reinen, *Inorg. Chem.* **25** (1986) 1650 (https://dx.doi.org/10.1021/ic00230a025)

101. E. Gamp, *ESR-Untersuchungen uber den Jahn-Teller-Effekt in oktaedrischen Kupfer(II)-Komplexen mit trigonalen dreizahnigen Liganden*, ETH, Zurich, 1980 (https://dx.doi.org/10.3929/ethz-a-000215808)

102. A. D. Liehr, *Z. Phys. Chem.* **9** (1956) 338 (https://dx.doi.org/10.1524/zpch.1956.9.5_6.338)

103. L. C. Snyder, *J. Chem. Phys.* **33** (1960) 619 (https://dx.doi.org/10.1063/1.1731211)

104. W. D. Hobey, A. D. McLachlan, *J. Chem. Phys.* **33** (1960) 1703 (https://dx.doi.org/10.1063/1.1731485)

105. R. Meyer, F. Graf, T. Ha, H. H. Gunthard, *Chem. Phys. Lett.* **66** (1979) 65 (https://dx.doi.org/10.1016/0009-2614(79)80370-X)

106. W. T. Borden, E. R. Davidson, *J. Am. Chem. Soc.* **101** (1979) 3771 (https://dx.doi.org/10.1021/ja00508a012)

107. C. Cunha, S. Canuto, *J. Molec. Struct THEOCHEM* **464** (1999) 73 (https://dx.doi.org/10.1016/S0166-1280(98)00536-3)

108. M. J. Bearpark, M. A. Robb, N. Yamamoto, *Spectrochim. Acta, A* **55** (1999) 639 (https://dx.doi.org/10.1016/S1386-1425(98)00267-4)

109. J. H. Kiefer, R. S. Tranter, H. Wang, A. F. Wagner, *Int. J. Chem. Kin.* **33** (2001) 834 (https://dx.doi.org/10.1002/kin.10006)

110. S. Zilberg, Y. Haas, *J. Am. Chem. Soc.* **124** (2002) 10683 (https://dx.doi.org/10.1021/ja026304y)

111. T. Ichino, S. W. Wren, K. M. Vogelhuber, A. J. Gianola, W. C. Lineberger, J. F. Stanton, *J. Chem. Phys.* **129** (2008) 084310 (https://dx.doi.org/10.1063/1.2973631)

112. D. Leicht, M. Kaufmann, G. Schwaab, M. Havenith, *J. Chem. Phys.* **145** (2016) 074304 (https://dx.doi.org/10.1063/1.4960781)

113. A. D. Liehr, *J. Phys. Chem.* **67** (1963) 389 (https://dx.doi.org/10.1021/j100796a043)

114. N. Iwahara, T. Sato, K. Tanaka, L. F. Chibotaru, *Phys. Rev., B* **82** (2010) 245409 (https://dx.doi.org/10.1103/PhysRevB.82.245409)

115. J. H. Ammeter, R. Bucher, N. Oswald, *J. Am. Chem. Soc.* **96** (1974) 7833 (https://dx.doi.org/10.1021/ja00832a049)

116. I. Utke, A. Gölzhäuser, *Angew. Chem. Int. Ed.* **49** (2010) 9328 (https://dx.doi.org/10.1002/anie.201002677)

117. M. Zlatar, M. Allan, J. Fedor, *J. Phys. Chem., C* **120** (2016) 10667 (https://dx.doi.org/10.1021/acs.jpcc.6b02660)

118. K. E. R. Marriott, L. Bhaskaran, C. Wilson, M. Medarde, S. T. Ochsenbein, S. Hill, M. Murrie, *Chem. Sci.* **6** (2015) 6823 (https://dx.doi.org/10.1039/C5SC02854J).